

## On the evolution of a solitary wave in a gradually varying channel

By PETER CHANG, W. K. MELVILLE  
 AND JOHN W. MILES

Institute of Geophysics and Planetary Physics, University of California,  
 San Diego, La Jolla, California 92093

(Received 16 February 1979)

The adiabatic approximation for a solitary wave in a channel of gradually varying breadth  $b$  and uniform depth is tested by experiment and by numerical solution of the generalized Korteweg–de Vries (KdV) equation. The results for a linearly diverging channel show good agreement with the prediction  $\alpha$  (dimensionless wave amplitude)  $\propto b^{-\frac{2}{3}}$ . The experiments and numerical solutions for the linearly converging channel show that the wave growth is well approximated by  $\alpha \propto b^{-\frac{1}{2}}$ . The discrepancy between the diverging and converging channels is shown to be due to nonlinear effects associated with the choice of the spatial variable as the slow variable in the generalized KdV equation. The measured and computed profiles display the predicted ‘shelves’ of elevation and depression in the converging and diverging channels, respectively.

### 1. Introduction

The free-surface displacement  $\eta(s, x)$  of a weakly nonlinear, weakly dispersive, unidirectional wave in a channel of gradually varying breadth  $b(x)$  and uniform depth satisfies the generalized Korteweg–de Vries (KdV) equation (Shuto 1974)

$$\frac{1}{6}\eta_{sss} + \frac{3}{2}\eta\eta_s + \eta_x + \frac{1}{2}(b'/b)\eta = 0, \quad (1.1)$$

where

$$s = x - t - x_0, \quad (1.2)$$

$x$  is a dimensionless, horizontal co-ordinate in a fixed reference frame, and  $t$  is a dimensionless time. The units of length and time are  $d$  and  $(d/g)^{\frac{1}{2}}$ , respectively, where  $d$  is the quiescent depth. The assumptions of weak nonlinearity, weak dispersion, and gradually varying breadth imply  $\alpha \ll 1$ ,  $\lambda \gg 1$  and  $\lambda|b'|/b \ll 1$ , respectively, where  $\alpha d$  and  $\lambda d$  are the amplitude and length scales of  $\eta$  (both  $\alpha$  and  $\lambda$  may depend on  $x$ ). Boussinesq scaling, which corresponds to a balance between nonlinearity and dispersion, implies  $\lambda = O(\alpha^{-\frac{1}{2}})$  and is henceforth implicit.

#### 1.1. Adiabatic approximation

The last term in (1.1), which represents the effect of channel variation on the evolution of  $\eta$ , is small compared with both the first (dispersion) and second (nonlinear) terms if  $|b'|/b \ll \alpha^{\frac{2}{3}}$ . The corresponding adiabatic approximation for a solitary wave is given by

$$\eta = \alpha \operatorname{sech}^2\left\{\frac{1}{2}(3\alpha)^{\frac{1}{2}}(s - \tau)\right\} \quad |b'|/b \ll \alpha^{\frac{2}{3}} \ll 1, \quad (1.3a)$$

where

$$\alpha = \alpha_0(b/b_0)^{-\frac{2}{3}}, \quad \tau = \frac{1}{2} \int_{x_0}^x \alpha dx, \quad (1.3b, c)$$

and the subscript zero implies evaluation at the reference station  $x_0$ . The trajectory of the wave peak in an  $x, t$  plane is given by  $s = \tau$ ; the corresponding wave slowness (reciprocal speed) is  $1 - \frac{1}{2}\alpha$ .

The primary purpose of the present paper is to report experimental and numerical tests of the approximation (1.3), especially (1.3*b*), for a channel that is either expanding or contracting linearly: either

$$b/b_0 = x/x_0 \quad \text{or} \quad b/b_0 = (x_1 - x)/(x_1 - x_0), \quad (1.4a, b)$$

where either  $x = 0$  or  $x_1$  is a virtual apex. Note that  $|b'|/|b| \ll \alpha^{\frac{2}{3}}$  implies either  $x$  or  $x_1 - x \gg \alpha^{-\frac{2}{3}}$ .

### 1.2. Secondary waves

The generalized KdV equation admits the integral invariants

$$I = b^{\frac{1}{2}} \int_{-\infty}^{\infty} \eta ds, \quad E = b \int_{-\infty}^{\infty} \eta^2 ds. \quad (1.5a, b)$$

$I$  may be termed a *pseudo mass invariant*, whilst  $E$  is a (true) energy invariant. A true measure of mass is

$$M = b \int_{-\infty}^{\infty} \eta ds = Ib^{\frac{1}{2}}, \quad (1.6)$$

which is not an invariant of (1.1) (unless the channel is uniform); this deficiency is a consequence of the neglect of the reflected wave, which necessarily is induced by the channel variation.

The adiabatic approximation (1.3) conserves  $E$  but neither  $I$  nor  $M$ . An approximate solution of (1.1) that conserves  $I$  may be obtained by adding to the primary wave (1.3*a*) a trailing secondary wave (its wave speed is 1, compared with  $1 + \frac{1}{2}\alpha$  for the primary wave),  $\eta_+$ , which is often designated as a 'shelf' (Kaup & Newell 1978; Ko & Kuehl 1978). The end result for a channel of linearly varying breadth is [the calculation follows Miles (1979), §4 and assumes that the wave originates at  $x = x_0$  and  $t = 0$ ]

$$\eta_+ = -\frac{4}{3}b'b^{-\frac{1}{2}}(3\alpha_0 b_0 + 2b's)^{-\frac{1}{2}}, \quad 0 < s < \tau = \frac{3}{2}\alpha_0(b_0/b')\{(b/b_0)^{\frac{1}{2}} - 1\}. \quad (1.7)$$

The length scale of  $\eta_+$  is that of the channel variation,  $b/|b'|$ , which is, by assumption, large compared with that of the primary wave, and (1.7) does not provide a detailed description in the neighbourhoods of the end points  $s = 0$  and  $s = \tau$ . Note that  $|\eta_+| \ll \alpha$  if, as assumed in (1.3),  $|b'|/b \ll \alpha^{\frac{2}{3}}$ .

An approximation that conserves  $M$ , and therefore goes beyond (1.1), may be obtained by adding a reflected wave,  $\eta_-$ , which recedes in the negative  $x$  direction with unit speed and also has the length scale of the channel variation (Miles 1979). For the primary wave (1.3), however,  $|\eta_-| \ll \alpha^2$ , which is too small for reliable measurement in the present context.

### 1.3. Green's-law approximation

The channel-variation term dominates the dispersion and nonlinear terms in (1.1) if  $|b'|/b \gg \alpha^{\frac{2}{3}}$ , and the counterpart of (1.3) then is (cf. Green's law)

$$\eta = \alpha \operatorname{sech}^2\{\frac{1}{2}(3\alpha_0)^{\frac{1}{2}}s\} \quad (\alpha^{\frac{2}{3}} \ll |b'|/|b| \ll \alpha^{\frac{1}{2}}), \quad (1.8a)$$

where 
$$\alpha = \alpha_0(b/b_0)^{-\frac{1}{2}}. \quad (1.8b)$$

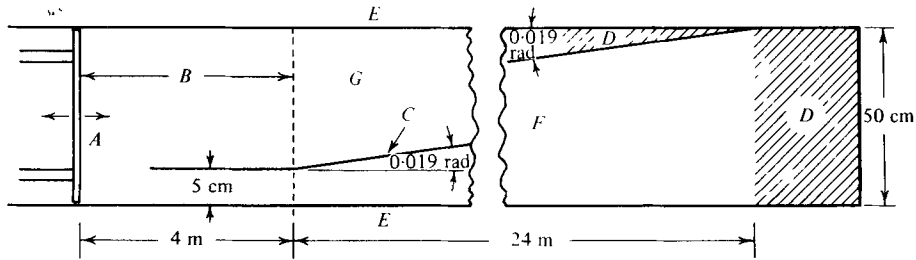


FIGURE 1. Plan view of the wave channel (not to scale). *A*, bulkhead wave-maker. *B*, entrance section. *C*, diagonal wall. *D*, wave-damping material. *E*, glass sidewalls. *F*, diverging channel. *G*, converging channel.

This approximation conserves both  $I$  and  $E$ , but not  $M$ . Conservation of  $M$  requires the addition of a reflected wave, just as with (1.3). It is worth emphasizing that both (1.3) and (1.8) satisfy the Korteweg-de Vries equation in the limit of a uniform channel ( $b/b_0 = 1$ ).

## 2. Experiments

The experiments were carried out in a glass wave channel 33 m long, 0.80 m deep and 0.50 m wide. The converging and diverging channels (of expansion angle 0.019 rad) were formed by a vertical wall running diagonally across the length of the channel, with a contiguous section of wall, parallel to the sidewalls, providing a uniform entrance section (figure 1). Great care was taken to seal and align the wall. Measurements of the channel width were made at one metre intervals and showed the departure from linear converging/diverging sections to be at most  $\pm 2$  mm ( $\pm 0.002$  rad).

Solitary waves were generated in the entrance section by a vertical bulkhead actuated by a servo-controlled hydraulic system. The horizontal displacement of the bulkhead corresponded to the horizontal displacement of a fluid particle in the solitary wave. This particle path was computed digitally, converted to an analogue signal, and recorded as a frequency-modulated signal on magnetic tape. This recording was subsequently used to drive the wave-maker. More complete details are given by Chang (1978).

The surface displacement was measured with resistance wave gauges having a resolution of  $\pm 0.02$  cm. Each gauge consists of two 0.0008 cm-diameter, stainless steel wires separated by 0.2 cm and stretched between insulators at the ends of a C-shaped aluminium frame. This frame is attached to a box-section beam which is supported between rollers and can be cranked up and down past a vernier scale. The parallel wires form one leg of an a.c. bridge, the output of which is an amplitude-modulated signal that is fed to a phase-locked demodulator. The final output in a d.c. voltage approximately proportional to the length of wire immersed.

The experimental procedure was as follows. The water surface was skimmed continuously overnight and the depth checked and adjusted immediately prior to beginning the experiment. The wave gauges were statically calibrated and the gain of the wave generator checked and adjusted to give the required wave amplitude. The solitary wave was generated a number of times, with the second gauge being moved through 1 to 2 m between runs. The time between runs was sufficient to ensure a

quiescent surface for the subsequent run. A typical experiment lasted from two to four hours, depending on whether one or two wave amplitudes were being generated. At the end of the series of experiments the gauges were calibrated a second time. The calibration curves were fitted by polynomials of up to 5th order with an r.m.s. error of less than 1 mm. There was some drift of the gauges between calibrations, for which reason the first (last) calibration was used for the first (last) half of the experiment. This procedure yielded a maximum calibration error at the crossover point. This error typically was in the range 2–5%, with a maximum error of 8%, corresponding in that particular case to only 0.05 cm.

In each case the mean of the first 100 words from each record was used as the datum from which the surface elevation was computed.

Experiments were conducted for water depths of 20, 30 and 40 cm and initial wave amplitudes in the range  $0.05 \leq \alpha \leq 0.4$ .

### 3. Numerical solutions

In the generalized KdV equation (1.1), it is expedient to choose  $x$ , rather than  $t$ , as the slow variable, since the breadth, or more specifically  $b/b'$ , is prescribed as a slowly varying function of  $x$ . In the linearly varying channel, however,  $b/b'$  is linear in  $x$ , by virtue of which this procedure is unnecessary; moreover, as we shall see below, it is less accurate than retaining  $t$  as the slow variable. Thus, the equation that was solved numerically is

$$\eta_t + \frac{1}{2}t^{-1}\eta + \frac{3}{2}\eta\eta_s + \frac{1}{6}\eta_{sss} = 0. \quad (3.1)$$

Equation (3.1) was solved by a pseudo-spectral method, splitting off the linear terms (Tappert 1974) and using a partially corrected, second-order, Adams–Bashforth scheme (Gazdag 1976) for the nonlinear term. The code is a simple modification of that used by Meiss & Pereira (1978). The stability of the method was tested by solving the Korteweg–de Vries equation with a Boussinesq profile as initial data. Over an evolution interval comparable with that of the solutions described below, mass and energy were conserved to better than one part in  $10^9$ , and the error in the wave amplitude was less than 0.05%.

For comparison with the measurements, the initial data corresponded to a Boussinesq profile having a maximum amplitude equal to that of the measured profile at the entrance to the converging/diverging section of the channel. As will become evident below, the measured departure from the Boussinesq profile at the entrance of the converging channel was generally small, with a difference of 2–3% of the wave amplitude at the leading and trailing edges of the wave; however, at the entrance to the diverging channel there was evidence of dispersion, perhaps due to viscous effects in the narrow entrance section (widening of the entrance section would have resulted in a corresponding reduction of the length of the diverging section, which was not considered desirable). The use of the measured profile as initial data for the numerical solution would have required an arbitrary truncation of the dispersive tail, making comparison of the finer features of the measurements and numerical solutions somewhat arbitrary.

In addition to specifying the initial profile, an initial time must be given. This is just the time taken for a linear wave to travel from the vertex of the channel to the initial position of the wave. In each case the wave had a positive velocity, whence the

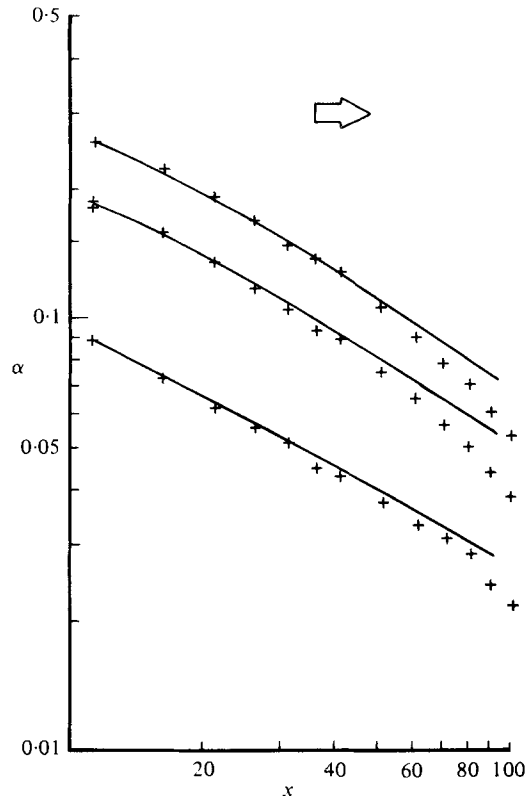


FIGURE 2. Measured (+) and computed (—) amplitudes,  $\alpha$ , of solitary waves in a diverging channel of expansion angle  $0.019$  rad and  $20$  cm depth. The initial amplitudes are  $\alpha_0 = 0.088, 0.185, 0.259$ . Note that  $\alpha$  and  $x$  are normalized with respect to the quiescent depth.

initial times for the diverging and converging channels were positive and negative, respectively, with the magnitude of the former being less than that of the latter.

#### 4. Results

A total of thirty-six experiments were conducted, ranging over both converging and diverging channels, the three water depths, and initial amplitudes in the range  $0.05 \leq \alpha \leq 0.4$ . We present only a selection of the measurements here. It should be noted that the level surface of static equilibrium subsequent to the paddle motion is elevated relative to the quiescent level used here; however, the relative increment in the water depth is at most  $0.016$  and leads to a negligible error in the linear wave speed. The horizontal position  $x$  is measured from the vertex of the channel and the waves in both the converging and diverging channels are considered to have a positive velocity. Thus the converging channel is defined in  $x \leq 0$  and the diverging channel in  $x \geq 0$ . This convection is denoted in the figures by a bold arrow indicating the direction of wave propagation.

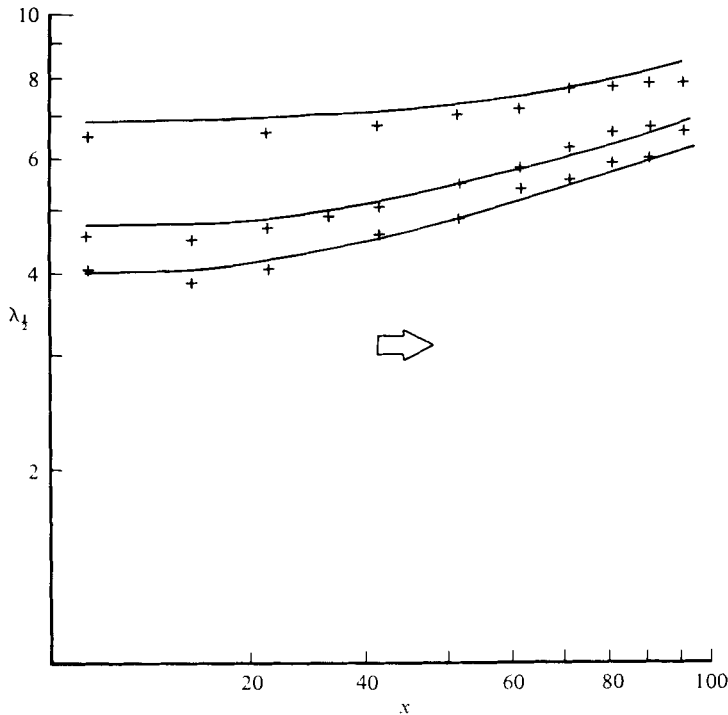


FIGURE 3. Measured (+) and computed (—) halfwidth,  $\lambda_{\frac{1}{2}}$ , corresponding to the amplitudes shown in figure 1.

#### 4.1. Amplitude and characteristic lengths

Figure 2 shows the wave amplitude *versus* position ( $\alpha$  vs.  $x$ ) for experiments in the diverging channel of 20 cm depth, along with the corresponding numerical results. This is the only depth of the diverging channel for which comparison with the numerical results is possible: for the larger depths, the position of the initial station,  $x_0$  was such that the initial profile would have extended to negative values of  $x$ . The differences between the measured and computed amplitudes are generally small and within the error estimates over most of the range of  $x$ . However, for large  $x$  the measured amplitudes decrease more rapidly than the numerical results, presumably in consequence of viscous dissipation (see appendix). This effect is more pronounced for the waves of larger amplitude. The numerical results show that the amplitude initially varies according to Green's law ( $\alpha \propto b^{-\frac{1}{2}}$ ), before tending towards the adiabatic approximation ( $\alpha \propto b^{-\frac{2}{3}}$ ). The transition from the  $-\frac{1}{2}$  to  $-\frac{2}{3}$  law shifts to lower values of  $x$  with increasing wave amplitude.

Figure 3 shows the measured and computed values of the dimensionless half-width  $\lambda_{\frac{1}{2}}$ , the distance between the points on the wave profile at which the amplitude is half of the maximum. This choice of a characteristic length of the wave is arbitrary. An alternative length might be defined by an integral of a moment of the wave profile; however, the non-conservation of mass of the model equation and the dissipation of energy in the experiments thwart such a choice. The difference between the measured initial half-width and that of the corresponding Boussinesq profile, based on the wave

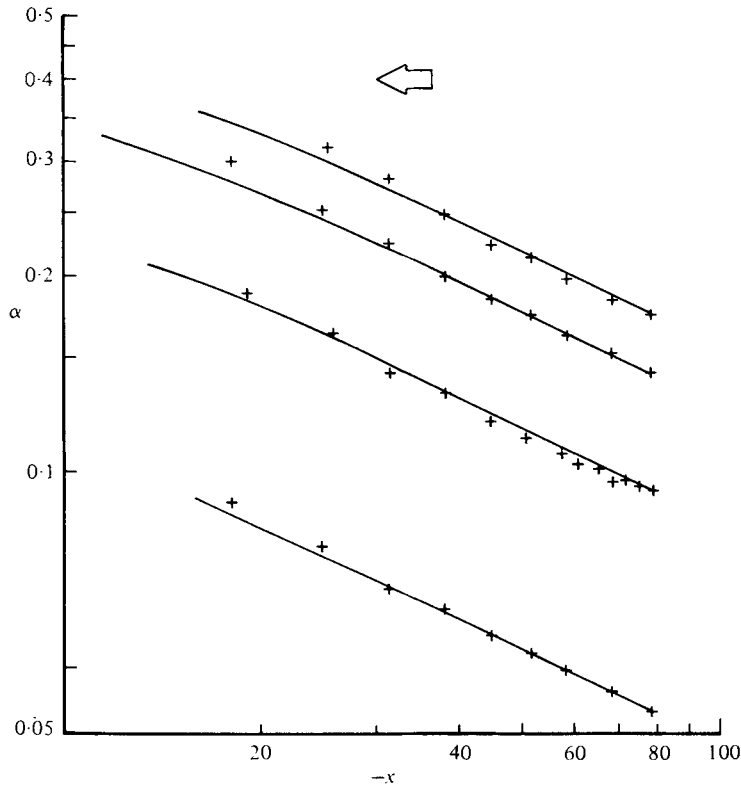


FIGURE 4. Measured (+) and computed (—) amplitudes of solitary waves in a converging channel of convergence angle 0.019 rad and 30 cm depth. The initial amplitudes are  $\alpha_0 = 0.043, 0.093, 0.140, 0.174$ .

amplitude, was at most 5%. The subsequent difference between the measured and computed lengths remained comparable with this initial error. The numerical solutions show that the half-length is initially constant and tends to a  $\frac{1}{3}$ -power law ( $\lambda_{\frac{1}{2}} \propto b^{\frac{1}{3}}$ ) with increasing  $x$ . These results, along with those of figure 2, are consistent with (1.3) and imply that any departures from the Boussinesq profile over the range of the experiment's were confined to those parts of the profile where the displacement was less than  $\frac{1}{2}\alpha$ .

Comparison between the measurements and numerical solutions was possible for all three depths of the converging channel; however, we shall present only the results for a depth of 30 cm. Figure 4 displays  $\alpha$  vs.  $x$  for  $h = 30$  cm. The agreement between the measured and computed amplitudes is good, the discrepancies being comparable with the estimated experimental error. The agreement for the other two depths was good at the smallest initial amplitude,  $\alpha_0 \simeq 0.05$ , but deteriorated as  $\alpha_0$  increased. This behaviour is not evident in figure 4. The measured amplitudes in each case correspond to  $\alpha \propto b^{-\frac{1}{2}}$  to within the expected error. In contrast, the numerical solutions tend to a lower slope as  $x$  decreases. These results contrast markedly with the predicted  $-\frac{2}{3}$ -power law, which discrepancy is accounted for below. The corresponding half-widths for the 30 cm depth are shown in figure 5. The agreement between the measurements and numerical results for  $\alpha_0 = 0.043$  is good, but considerable discrepancy

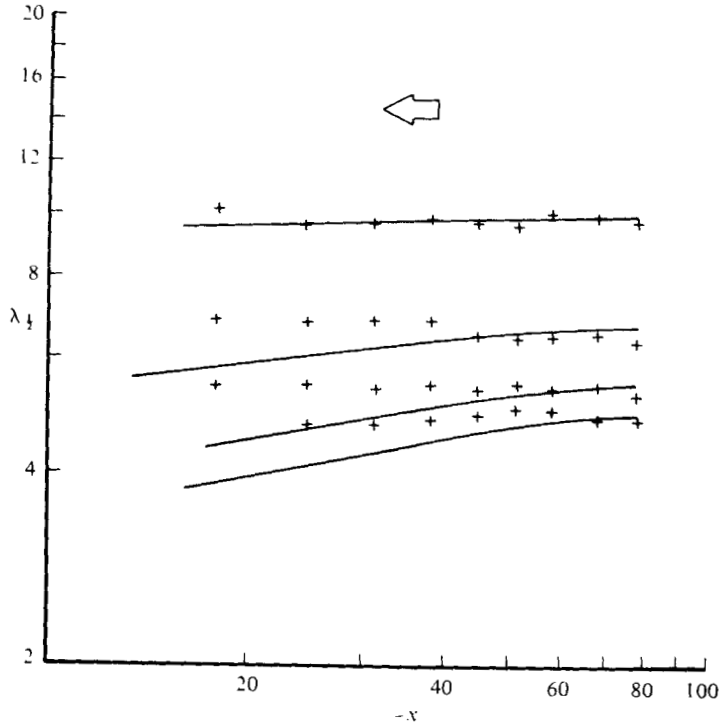


FIGURE 5. Measured (+) and computed (—) halfwidths corresponding to the amplitudes shown in figure 4.

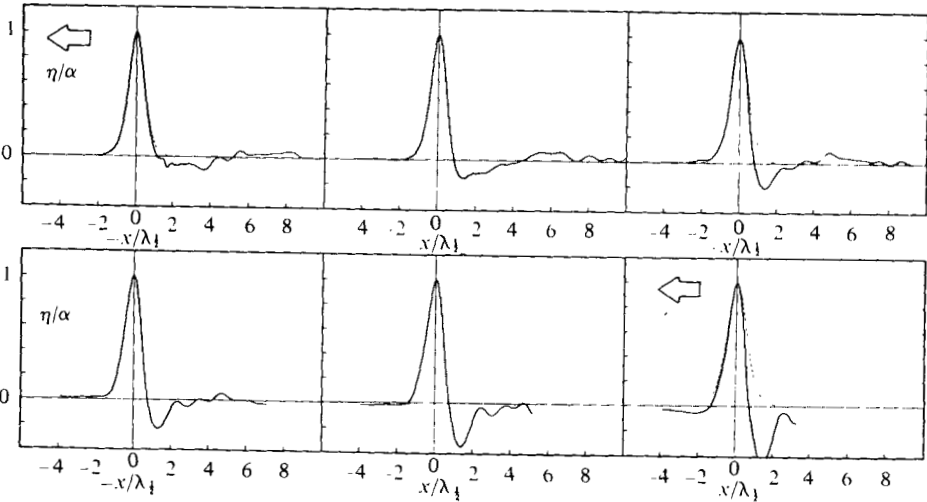


FIGURE 6. Measured temporal profiles (—) and Boussinesq profiles (---) for  $\alpha_0 = 0.4$  in a diverging channel of 30 cm depth. The profiles were measured at  $x = 4.2, 17.6, 30.9, 37.6, 50.9, 64.3$ .

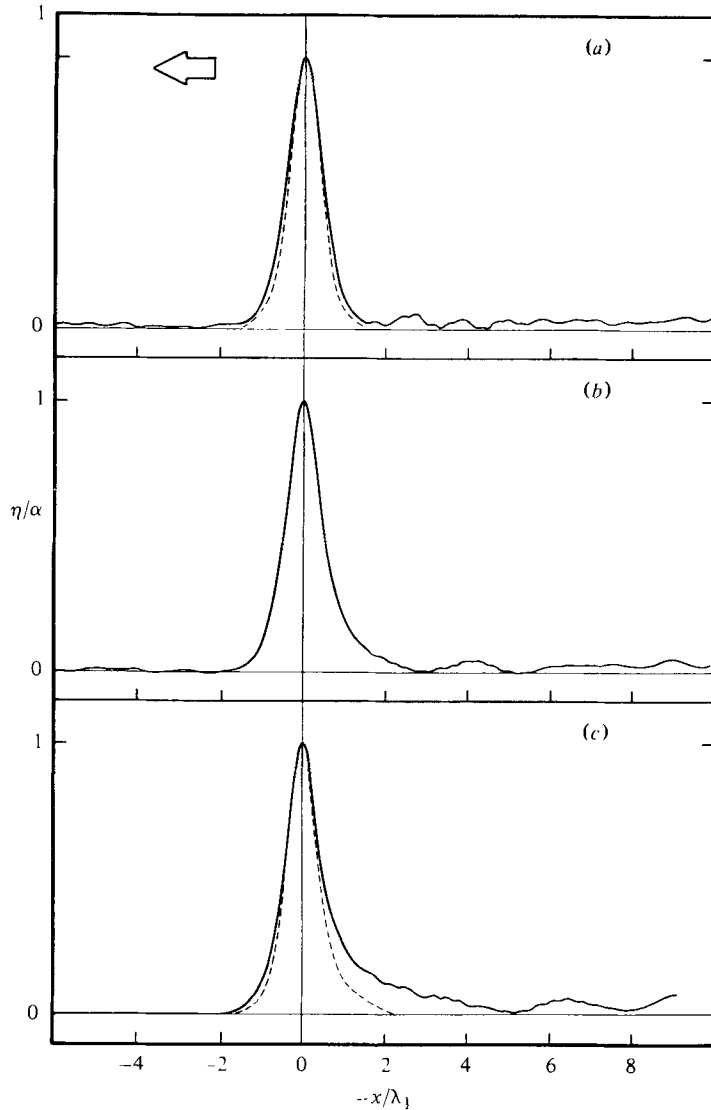


FIGURE 7. Measured normalized profiles of a solitary wave of initial amplitude  $\alpha_0 = 0.2$  in a converging channel of 40 cm depth at stations (a)  $x_0 = -58.5$ , (b)  $x = -43.5$ , (c)  $x = -23.5$ . The broken lines in (a) and (c) show the corresponding initial data and subsequent numerical solution of equation (3.1).

occurs at larger amplitudes. The measurements show that  $\lambda_{\frac{1}{2}}$  is approximately constant, whereas the numerical solutions show  $\lambda_{\frac{1}{2}}$  decreasing as the amplitude increases.

#### 4.2. Wave profiles

The departure from the Boussinesq profile that is indicated by the above results is illustrated in figures 6 and 7, where the normalized temporal profiles of the evolving wave are shown. Figure 6 shows a wave of  $\alpha_0 = 0.39$  evolving in a diverging channel of depth 30 cm. The corresponding Boussinesq profile is shown at selected stations.

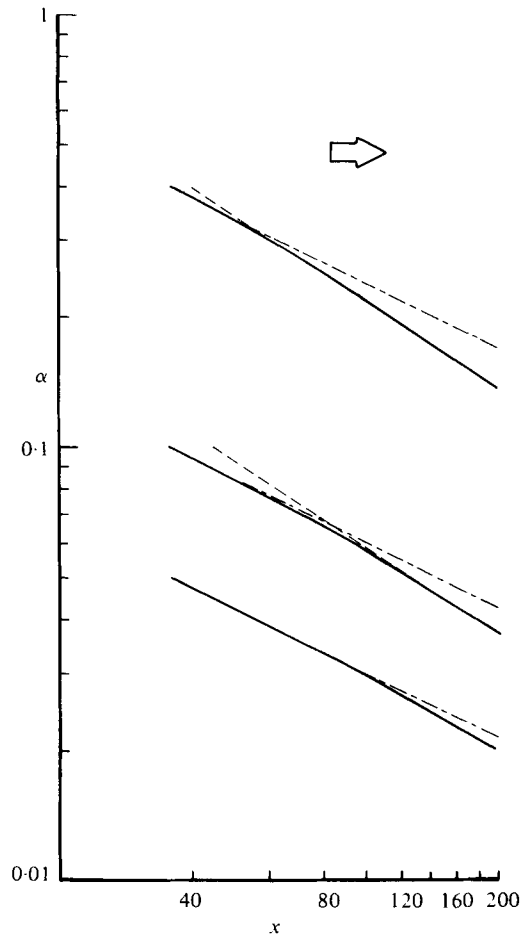


FIGURE 8. Amplitude *vs.* position ( $\alpha$  *vs.*  $x$ ) of computed profiles of solitary waves of amplitude  $\alpha_0 = 0.05, 0.1, 0.4$  in a diverging channel:  $t_0 = 36$ . Also shown are the lines of slope  $-\frac{1}{2}$  (---),  $-\frac{2}{3}$  (----).

Initially the two profiles agree very well except at the tail of the main wave, where a depression of up to 10% of the wave amplitude exists in the measured profile. Further development of this depression takes place over the central portion of the channel, whereas the leading face of the wave agrees very well with the Boussinesq profile. Towards the end of the channel there also is evidence of an evolving depression leading the wave. This feature was evident in other experiments in the diverging channel but did not appear in the converging channel.

Figure 7 shows a wave of  $\alpha_0 = 0.2$  evolving in a converging channel of depth 40 cm. Here we see that the initial profile is longer than the corresponding Boussinesq form; however, it is almost coincident with the normalized  $\text{sech}^2$  profile† and has only a small trailing wake. As the wave evolves, it trails a positive shelf that grows in time. A

† The normalized  $\text{sech}^2$  profile has two independent parameters: the amplitude and half-width. This contrasts with the Boussinesq profile for which there exists a functional relationship between the amplitude and half-width.

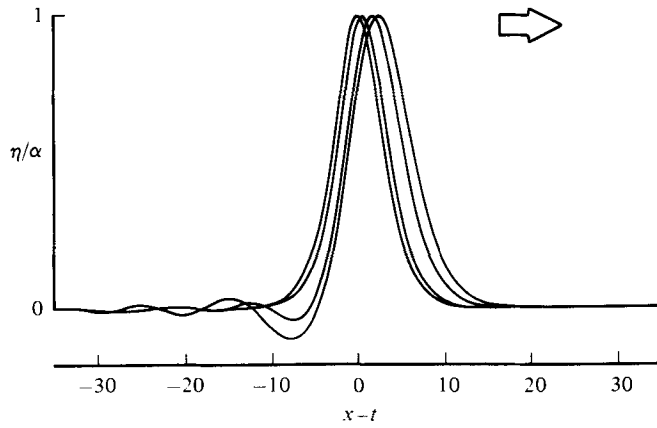


FIGURE 9. Computed, normalized profiles shown as a function of  $s$  at times  $t = 26, 51, 101, 151$  (from left to right) for a wave of amplitude  $\alpha_0 = 0.1$  in a diverging channel (cf. figure 8).

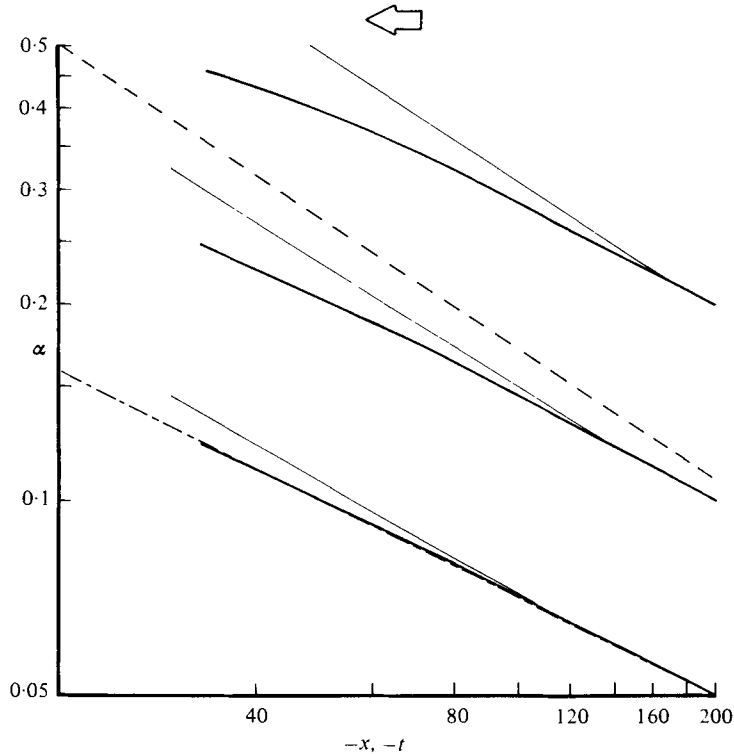


FIGURE 10. Amplitude  $\alpha$  vs. position  $x$  (—) and time  $t$  (—) of computed profiles of solitary waves of amplitude  $\alpha_0 = 0.05, 0.1, 0.2$  in a converging channel:  $x_0 = t_0 = 200$ . Also shown are lines of slope  $-\frac{1}{2}$  (-·-), and  $-\frac{2}{3}$  (- - -). Note the increasing divergence of the temporal and spatial curves with increasing wave amplitude.

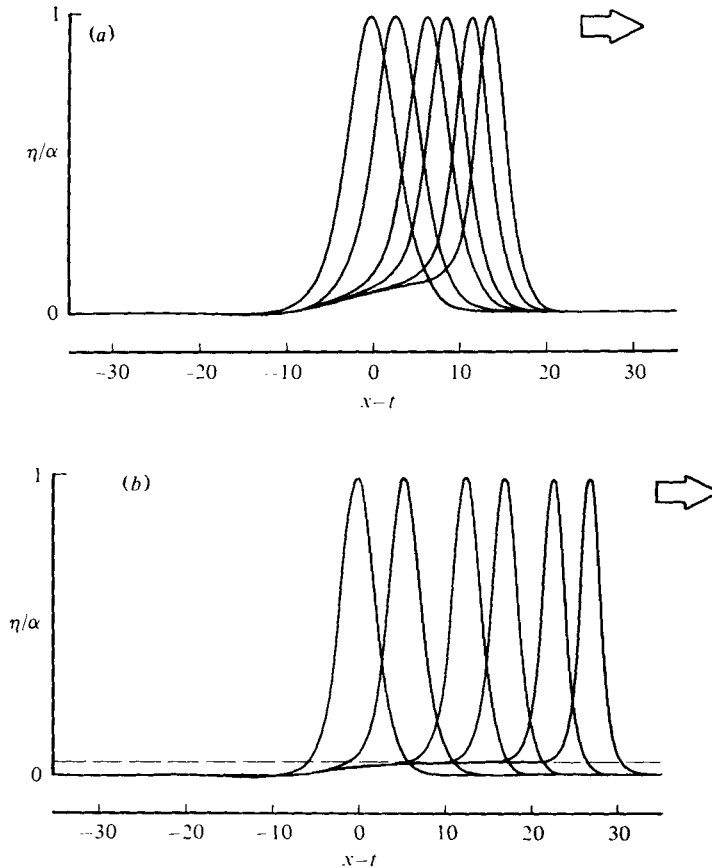


FIGURE 11. Computed, normalized profiles shown as a function of  $s$  at times  $t = -200, -150, -100, -75, -50, -35$  (from left to right) for waves of amplitude (a)  $\alpha_0 = 0.1$ , (b)  $\alpha_0 = 0.2$ . The broken line in (b) is the amplitude of the shelf predicted by equation (1.7) (cf. figure 10). [It should be noted that the amplitude of the shelf predicted by (1.7) varies as  $b^{-1}$  and that the amplitude used to normalize these profiles (cf. figure 10) differs negligibly from the  $-\frac{1}{2}$ -power law over most of the range shown here. The maximum difference (of approximately 6% at  $t = -35$ ) is not discernible on the scale of this figure.]

profile obtained from the numerical solution using the initial measured amplitude and a Boussinesq profile also is shown in figure 7 and indicates that the evolution of the tail is more rapid in the experimental results. It should be remarked that this is consistent with the neglect of the reflected wave.

#### 4.3. Additional numerical results

Some features of the evolution of the solitary wave that are found in the experiments may be further investigated by numerical solutions, which permit development of the wave over longer periods.

Figure 8 shows the evolution of the wave amplitude in a diverging channel with  $\alpha_0 = 0.05, 0.1, 0.4$  at  $x_0 = 36$ . The predominant feature of these curves is that they evolve initially according to Green's law, before tending towards the predicted  $-\frac{2}{3}$ -power law. The evolution of the normalized wave profile for  $\alpha_0 = 0.1$  in a

reference frame moving from left to right with the linear wave velocity is shown in figure 9; it displays the dispersive wave train trailing the primary wave of elevation. The maximum amplitude of the depression, predicted by (1.7) (setting  $s = 0$ ), was found to be an order of magnitude larger than that of the numerical solution. The reason for this discrepancy is not clear at this time.

Figure 10 shows the evolution of the wave amplitude in a converging channel with  $\alpha_0 = 0.05, 0.1, 0.2$  at  $x_0 = -200$ . In this case the amplitude is plotted against both the position and time. As in the diverging channel for small time, the amplitude initially varies according to Green's law; however, the transition to the  $-\frac{2}{3}$ -power law does not occur in the space domain, and Green's law remains a good approximation over most of the range of the simulation. In the time domain the expected transition does occur and is more rapid for the larger waves. The evolution of the normalized profiles for  $\alpha_0 = 0.1, 0.2$  is shown in figure 11. Comparison of the profiles shows that the shelf evolves more rapidly with increasing amplitude of the primary wave. The maximum amplitude of the shelf computed from (1.7) ( $s = 0$ ) also is shown in figure 11(b) and agrees well with the amplitude of the plateau.

## 5. Discussion

The experiments and the numerical solutions imply that the adiabatic approximation (1.3) is good for the diverging channel, but poor for the converging channel. In each case the Green's-law approximation (1.8) has been found to be valid for initial wave amplitudes considerably in excess of the expected range of validity.

The reason for the departure from the  $\frac{2}{3}$ -power law in the converging channel is made apparent by the numerical results in figure 10. Whereas the temporal dependence of the amplitude is according to (1.3b), the increasing wave amplitude leads to an increasing wave speed, such that the linear transformation between the spatial and temporal variables is no longer a good approximation. Thus the spatial and temporal curves diverge, as is clear from the figure. In contrast, in the diverging channel the wave speed approaches the linear value with the decreasing wave amplitude.

The extended validity of Green's law for describing the initial evolution of the wave amplitude is associated with the initial profiles (data) in the experiments (numerical solutions). In both cases they were, to a good approximation, Boussinesq profiles. By expanding  $\eta_t$  about the initial position  $(x_0, t_0)$  and using the initial data, it can be shown that for small  $(x - x_0, t - t_0)$  the wave amplitude,  $\alpha$ , is proportional to  $t^{-\frac{1}{2}}$ .

We wish to thank our colleagues at the Hydraulics Laboratory, Scripps Institution of Oceanography, for their help in conducting the experiments. Jim Meiss and Nino Pereira generously let us use their spectral code. This work was supported by the Physical Oceanography Division, National Science Foundation (NSF Grant OCE77-24005), by a contract with the Office of Naval Research, and by a computing grant from the National Center for Atmospheric Research, which is funded by the National Science Foundation.

### Appendix. Boundary-layer damping

Boundary-layer damping of a solitary wave in a gradually varying channel may be calculated from the result (cf. Miles 1976)

$$(d/dx) \left\{ b(gd)^{\frac{1}{2}} \int_0^{\infty} |N(\omega, x)|^2 d\omega \right\} = -2b\delta \int_0^{\infty} \omega^{\frac{1}{2}} |N(\omega, x)|^2 d\omega, \quad (\text{A } 1)$$

where 
$$N(\omega, x) = \int_{-\infty}^{\infty} e^{-i\omega s} \eta(x, s) ds, \quad (\text{A } 2)$$

$$\delta = (\nu/8)^{\frac{1}{2}} d^{-1} \{1 + 2(d/b) + \mathcal{C}\}, \quad (\text{A } 3)$$

$\nu$  is the kinematic viscosity,  $\mathcal{C}$  is a surface-contamination parameter (the value of which is typically close to 1), and all quantities now are dimensional. Substituting the dimensional counterpart of (1.3) into (A 2) and then simplifying (A 1) yields

$$(d/dx) (a^{\frac{3}{2}} b) = -1.4232g^{-\frac{1}{2}} d^{-1} \delta a^{\frac{1}{2}} b, \quad (\text{A } 4)$$

wherein  $a \equiv \alpha d$ . Integrating (A 4) from  $x = x_0$  and invoking  $b' = \text{constant}$  yields

$$\frac{\alpha}{\alpha_0} = \left(\frac{b}{b_0}\right)^{-\frac{3}{2}} \left(1 + \frac{0.1007\epsilon^{\frac{1}{2}}}{b'} \alpha_0^{\frac{1}{2}} \left[ (1 + \mathcal{C}) \frac{b_0}{d} \left\{ \left(\frac{b}{b_0}\right)^{\frac{1}{2}} - 1 \right\} + 10 \left\{ 1 - \left(\frac{b}{b_0}\right)^{-\frac{1}{2}} \right\} \right] \right)^{-4}, \quad (\text{A } 5)$$

where 
$$\epsilon = (gd^3)^{-\frac{1}{2}} \nu. \quad (\text{A } 6)$$

It follows from (A 5) that the amplitude in the diverging channel is ultimately limited by viscosity and has the limiting value

$$\alpha \sim 10^{-4} \epsilon^{-2} (1 + \mathcal{C})^{-4} (db'/b)^4 \quad (b \uparrow \infty). \quad (\text{A } 7)$$

The limit  $b \downarrow 0$  for the converging channel is nugatory in consequence of the implicit assumption that the boundary-layer thickness is small compared with  $b$  [indeed, (A 5) is singular for a small, positive value of  $b$ ].

### REFERENCES

- CHANG, P. 1978 The solitary wave in a channel of varying width. M.S. Dissertation, University of California, San Diego.
- GAZDAG, J. 1976 Time-differencing schemes and transform methods. *J. Comp. Phys.* **20**, 196–207.
- KAUP, D. J. & NEWELL, A. C. 1978 Solitons as particles, oscillators, and in slowly changing media: a singular perturbation theory. *Proc. Roy. Soc. A* **361**, 413–446.
- KO, K. & KUEHL, H. H. 1978 Korteweg–de Vries soliton in a slowly varying medium. *Phys. Rev. Lett.* **40**, 233–236.
- MEISS, J. D. & PEREIRA, N. A. 1978 Internal wave solitons. *Phys. Fluids* **21**, 700–702.
- MILES, J. W. 1976 Damping of weakly nonlinear shallow-water waves. *J. Fluid Mech.* **76**, 251–257.
- MILES, J. W. 1979 On the Korteweg–de Vries equation for a gradually varying channel. *J. Fluid Mech.* **91**, 181–190.
- SHUTO, N. 1974 Non-linear long waves in a channel of variable section. *Coastal Engng in Japan* **17**, 1–12.
- TAPPERT, F. 1974 Numerical solutions of the Korteweg–de Vries equation and its generalisations by the split-step Fourier method. In *Nonlinear Wave Motion* (ed. A. C. Newell). Providence, R.I.: American Mathematical Society. *Lectures in Applied Mathematics*, vol. 15, pp. 215–216.